PCCP

ARTICLE TYPE

Cite this: DOI: 00.0000/xxxxxxxxxx

Benchmarking the performance of the newly designed K-band instrument with the conformationally rich amino alcohol isoleucinol

Mariyam Fatima [a,b], Cristóbal Pérez [a,b], Benjamin E. Arenas [a,b], Melanie Schnell [a,b*], and Amanda L. Steber [a,b,c*]

Received Date
Accepted Date

DOI: 00.0000/xxxxxxxxxx

Isoleucinol, a potential precursor to the essential α -amino acid isoleucine, has been studied using microwave spectroscopy from 2-26 GHz. The measurements between 18-26 GHz were performed with a newly developed segmented chirped-pulse Fourier transform microwave spectrometer, which has reduced the cost of the instrument by half compared to a direct excitation and detection chirped-pulse microwave spectrometer in the same frequency range. The performance of the instrument has been demonstrated and found to be comparable to the previous design. For isoleucinol, the flexibility of the *sec*-butyl side chain (R = -$CH(CH_3)CH_2CH_3$) can result in more than 200 different conformers from its five dihedral angles; however, experimentally, seven conformers have been assigned. A fit including the hyperfine splitting due to nitrogen nuclear quadrupole coupling for the rotational transitions is reported for all of the conformers, along with the experimental structures of the two lowest energy conformers. The observed conformers have intramolecular N···H-O hydrogen bond interactions, similar to the second energetically favorable conformer of the analogous amino acid, isoleucine. A complete linelist has been provided to facilitate a search for isoleucinol in the interstellar medium.

1 Introduction

More than 200 molecules have been detected in the interstellar medium (ISM) and circumstellar environments thus far[1,2]. This total does not include the number of various isotopologues that have been identified, for example, species containing D, ^{13}C, ^{18}O, ^{15}N, etc. The discovery of a majority of these interstellar species has been achieved from an interplay between laboratory rotational spectroscopy and radio-astronomical observations of their rotational emission in the microwave to submillimeter parts of the electromagnetic spectrum[3,4]. In addition to identifying the molecular makeup of a targeted area, these observations have also been used to determine the physical conditions in regions of the ISM and the factors that may have affected prebiotic chemistry on Earth[3–7]. The discovery of glycolaldehyde (the simplest sugar) in Sgr B2(N)[8] and glycine (the simplest amino acid) on comet 67P[9] indicates that these and other similar molecules could have formed in the ISM or circumstellar environments and then been transported to Earth. Therefore, the detection and chemistry involving prebiotic and biotic molecules, such as amino acids, sugars and amides, are an important focus for astronomers. Despite many attempts over the years[10–14], amino acids have yet to be detected in the ISM. This has led to questions about the chemistry necessary to produce them in these environments. The Miller-Urey experiment[15] illustrated that amino acids can be synthesized through the electrical discharge of methane, ammonia, water and hydrogen. While all of these components have been found to be present in interstellar and circumstellar environments, their densities compared to those in the Miller-Urey experiment would indicate that this would not be a viable formation pathway for the production of amino acids. A theoretical study on the formation of glycine points towards a barrierless reaction that could proceed in these cold, low density environments between ammonium ylide (C-$H_2N^+H_3$) and carbon dioxide[16]. In the same study, the authors found that ammonium ylide can also react exothermically with $HOCO^+$, HNCO, or HCHO to produce protonated glycine, glycinamide and the amino alcohol glycinol. In the case that an amino acid's alcohol counterpart is present in the ISM, it would be feasible to consider the formation of the acid from the oxidation of the alcohol with an oxidizer such as the OH radical. With this in mind, the detection of amino alcohols could lead to the detection of amino acids and provide some insight into

[a] *Deutsches Elektronen-Synchrotron (DESY), Notkestraße 85, 22607 Hamburg, Germany.*
[b] *Christian-Albrechts-Universität zu Kiel, Max-Eyth-Straße 1, 24118 Kiel, Germany.*
[c] *The Hamburg Centre for Ultrafast Imaging at Universtät Hamburg, Luruper Chaussee 149, 22761 Hamburg, Germany.*
[*] *Corresponding authors. E-mails: melanie.schnell@desy.de, amanda.steber@desy.de*
† Electronic Supplementary Information (ESI) available: [details of any supplementary information available should be included here]. See DOI: 10.1039/cXCP00000x/

potential chemical reaction pathways.

As already mentioned, laboratory rotational spectroscopy is one of the key techniques for characterizing molecules that could be present in the ISM. Fourier transform microwave (FTMW) spectroscopy is a powerful technique that is able to distinguish between different conformers, complexes, and isotopologue species. It is highly sensitive and gives molecular rest frequencies with high accuracy. The advancement of modern day electronics enabled the invention of the broadband chirped-pulse method in 2006[17] and broadened the horizon of the application of FTMW spectroscopy. Using chirped-pulse Fourier transform microwave (CP-FTMW) spectroscopy, it is possible to record rotational spectra of complex, flexible molecules spanning several gigahertz (GHz) of bandwidth within a few microseconds, where the information on all possible conformers or complexes are incorporated into a single spectrum. However, in high-frequency regions, like the millimeter or submillimeter range, the availability and cost of electronics become a challenge. Further advancements in technology have allowed for the integration of the CP-FTMW technique in high-frequency regions with the introduction of the segmented chirped-pulse method[18,19]. This method has been shown to maintain the resolution and sensitivity that one would expect of the CP-FTMW technique, while allowing for cheaper components to be utilized in the design. Using the state-of-the-art in technology, the implementation of the segmented approach has been incorporated into the design and construction of a spectrometer in the microwave 18-26 GHz region.

A number of small amino alcohols ($NH_2(CH_2)_2OH$-R), which can also serve as amino acid (NH_2CH_2CHO-R) precursors, such as glycinol[20] (R = H), alaninol[21] (R = CH_3) and serinol[22] (CH_2OH), have been studied via rotational spectroscopy. In these studies, their structures were determined and intramolecular interactions analyzed. Other small amino alcohols, valinol (R = $CH(CH_3)_2$), leucinol (R = $CH_2CH(CH_3)_2$), and alaninol, have been covered in a parallel study[23]. For all of the small amino alcohols, the conformational behavior is primarily governed by the intramolecular hydrogen bonding between the hydrogen atom of the hydroxyl group and the lone pair of the nitrogen atom (N$\cdots$H-O). In the study presented here, the next larger amino alcohol isoleucinol (R = $CH(CH_3)CH_2CH_3$) is investigated.

In this work, we present our study on the amino alcohol isoleucinol using CP-FTMW spectroscopy from 2-26 GHz. This frequency region overlaps with many large radio observatories, for example, the Jansky Very Large Array (JVLA), the Radio Telescope Effelsberg, and the Australian Square Kilometer Array Pathfinder (ASKAP) observatories, meaning the data we present can be used in observational searches for this astrochemically interesting molecule. Using the cold and isolated conditions of a molecular jet, we have identified low-lying ground state conformers of isoleucinol and, where applicable, obtained their structural information. The design and operation of the newly-built broadband 18-26 GHz spectrometer is also presented, and its performance is demonstrated in this work by the identification of the different conformers of isoleucinol arising from its flexible side chain R = $CH(CH_3)CH_2CH_3$.

2 Experimental and Computational Details

In the measurements of isoleucinol, the spectra between 2-26 GHz were studied under supersonic expansion conditions, yielding a molecular rotational temperature of $\sim$2 K. The entire frequency range was measured in three bands: 2-8 GHz, 8-18 GHz, and 18-26 GHz. The Hamburg COMPACT spectrometer, which is a CP-FTMW spectrometer with direct excitation and detection capabilities, was used for the 2-8 GHz measurements[24,25]. Recent upgrades have extended the measurement capabilities of the Hamburg COMPACT spectrometer to cover 8-18 GHz. For the 18-26 GHz range, a newly designed segmented CP-FTMW instrument was used. This new design is meant to decrease the total cost of the instrument. The performance of this instrument is demonstrated using hexanal, previously studied by Seifert et al.[26], and will be discussed in detail. These instruments are described later in this section.

L-isoleucinol (stated purity $\geq$ 97%), also known as (2S,3S)-2-amino-3-methylpentan-1-ol, was purchased from Fisher Scientific and used without further purification. The molecules were seeded into the supersonic expansion using a pulsed nozzle (Parker General Valve, Series 9) equipped with a heatable reservoir. The reservoir was heated to 45 °C, and neon was used as a carrier gas. To obtain an optimal signal, the backing pressure of neon in the COMPACT spectrometer was 3 bar, and in the 18-26 GHz instrument it was 1 bar. The backing pressure differs because the pumping efficiency is different for the two instruments. For the performance based measurements of the 18-26 GHz spectrometer, hexanal (stated purity 98%) was purchased from Alfa Aesar and used without further purification. A 0.2% hexanal in neon mixture was supersonically expanded using a pulsed nozzle with 1 bar backing pressure.

For isoleucinol, a total of 4.2 million (2-8 GHz), 1 million (8-18 GHz), and 2.9 million (18-26 GHz) free induction decays (FIDs) were co-added. The FIDs were Fourier transformed with a Kaiser-Bessel window function (α = 8) to give the broadband rotational spectra in the frequency domain.

All of the spectra were first fit using the JB95[27] and PGOPHER programs[28]. The presence of ^{14}N in isoleucinol, which has a nuclear spin I = 1, results in hyperfine structure in the rotational transitions because of the nuclear quadrupole interaction with the surrounding electric field. This interaction is dependent on variations in molecular symmetry, geometry and the electric environment. A refined fit including the nitrogen quadrupole coupling parameters was performed with the SPFIT program[29,30]. To determine the experimental structures and evaluate structural parameters, the KRA program – yielding the r_s structure[31], the STRFIT program providing the least squares fit (r_0) structure[32], and the EVAL program calculating the bond parameters[29], were used, all of which are available on the PROSPE website[33].

The conformational search for isoleucinol was performed using the semi-empirical method Austin Model 1 (AM1) and the Parametrized Models 3 and 6 (PM3 and PM6) as implemented in Spartan[34]. The resulting structures were then optimized with the B3LYP-D3(BJ) (Becke, three-parameter, Lee–Yang–Parr) exchange–correlation functional[35], including Grimme's empirical

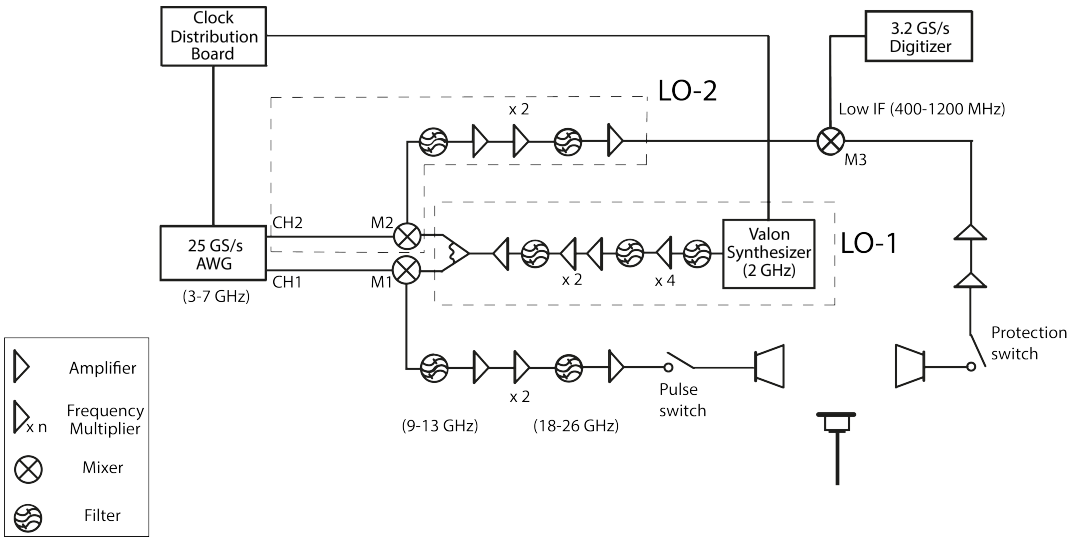

Fig. 1 Schematic of the 18-26 GHz segmented CP-FTMW spectrometer in Hamburg.

dispersion correction with Becke Johnson damping[36,37], and the def2-TZVP basis set[38] using Gaussian 09[39]. A total of seven structures were obtained with an energy difference of less than 6 kJ mol^{-1} from the global minimum. These structures were then re-optimized at B3LYP, using the aug-cc-pVTZ basis set[40–42].

In the following, the two different spectrometers are described in more detail:

2.1 Hamburg COMPACT Spectrometer (2-18 GHz)

2.1.1 2-8 GHz

In the 2-8 GHz range of the COMPACT spectrometer[24,25], the chirped pulses are generated by a 24 GS/s arbitrary waveform generator (Tektronix AWG 7122C) and amplified with an adjustable 300 W travelling wave tube amplifier (TWTA). A series of eight, 4 μs long microwave chirps spanning 2-8 GHz are broadcast into the vacuum chamber with a horn antenna (Q-par Angus WBH 2-18-NHG) to polarize the molecules. The horn antennae operate between 2-18 GHz, which has allowed us to extend the range of the spectrometer. Following each excitation, 40 μs of the FID are collected, giving a frequency resolution of ∼25 kHz, and recorded on a ∼100 GS/s oscilloscope (Tektronix DPO 72004C). The oscilloscope has an adjustable digitization rate, and it is set to 25 GS/s for the 2-8 GHz experiments. The fast frame option available on the oscilloscope allows for the collection of eight FIDs per gas pulse. In the present setup, the fast-frame approach can be performed together with a gas pulse repetition rate of 9 Hz, giving an effective repetition rate of 72 Hz.

2.1.2 8-18 GHz

For the 8-18 GHz extension, a series of eight chirped pulses of 2 μs duration are generated by the same AWG as used in the 2-8 GHz setup. These pulses span in frequency between 4-9 GHz, and they are subsequently up-converted. The entire frequency range is divided into four portions, which are measured independently of one another, and the up-converted frequencies are 8-10.5 GHz, 10.5-13 GHz, 13-15.5 GHz, and 15.5-18 GHz. The bandwidth is divided so that the power per GHz distribution using our 50 W solid state amplifier (SSA) better matches that which can be found in 8-18 GHz spectrometers[17,43] where a 300 W power amplifier is used. The use of the SSA was chosen to reduce the cost of the amplifying source.

The series of pulses from the AWG is amplified (Minicircuits, ZX60-123LN-S+) and doubled to between 8-18 GHz (ECLIPSE MICROWAVE, Model D2010LZ1). The doubler multiplies the bandwidth of the chirp by two without changing the pulse duration. The intermediate amplification step after the AWG is necessary to meet the minimum power requirements of the doubler. The pulses are then amplified with the 50 W SSA (Mercury Systems, L0618-46-T680). Each portion of the frequency range is collected for the desired number of averages before moving to the next portion. In a similar setup to the 2-8 GHz range, the molecules in each gas pulse are polarized with the series of pulses, and the FIDs are recorded on the oscilloscope. The digitization rate for this frequency range is set to 50 GS/s. The FIDs are collected for 20 μs yielding a frequency resolution of ∼50 kHz. Due to the limitations on the memory of the oscilloscope at high digitization rate, it is not possible to run the experiments at an effective repetition rate of 72 Hz, as in the 2-8 GHz setup. The maximum repetition rate of the gas pulse is set to 4 Hz, and with eight frames an effective repetition rate of 32 Hz is achieved.

To speed up the data collection, the experiments were performed in three steps as opposed to four. They are 8-13 GHz, 13-15.5 GHz, and 15.5-18 GHz. The signal intensity in the 8-13 GHz region was found to be sufficient to observe all the transitions lying in this range.

2.2 18-26 GHz Spectrometer

The schematic for the segmented CP-FTMW 18-26 GHz instrument is shown in Fig. 1. The instrument achieves phase stability by using the internal 10 MHz reference temperature compensated crystal oscillator (TCXO) of the Valon synthesizer. The design of the instrument is based on a combination of the segmented ap-

proach[18,19] and a multi-train setup, which is much like the fast frame configuration used for other CP-FTMW spectrometers, including the COMPACT[25]. In the segmented approach, the entire bandwidth of the spectrometer is divided into small chirped-pulse segments. The concatenation of these pulses is called a pulse train[18,19]. The replication of this pulse train in the memory of the AWG allows for the implementation of the multi-train technique, in which a series of pulse trains can be acquired in one gas pulse. More information on this can be found in the Supplementary Material. One channel (CH1) of a dual channel 25 GS/s per channel AWG is used to create the pulse trains in which ten 400 MHz chirped pulses span the 7-3 GHz range. Each chirped pulse is 1.5 μs long. These chirps are then frequency up-converted to 9-13 GHz with a 16 GHz local oscillator (LO-1) and doubled to 18-26 GHz. The doubling stage doubles not only the frequency but also the bandwidth of the pulse. Each 800 MHz segmented chirp is amplified using a 6 W SSA. The SSA has an internal switch which blocks noise transmission after the passing of the chirped pulse; however, it has a pulse modulation TTL time of 2 μs. The optimal pulse duration for this frequency range has been found to be 1.5 μs, and thus, a high power capacity Single-Pole Single-Throw (SPST) switch is used after the SSA to block the residual noise. The amplified chirps are then broadcast into the vacuum chamber with a horn antenna. For each gas pulse, a series of three pulse trains polarized the molecular ensemble. The multi-train setup was performed in conjunction with a gas pulse repetition rate of 10 Hz, giving an effective repetition rate of 30 Hz. The repetition rate of the instrument is mainly limited by the pumping speed. The spectrometer achieves vacuum through turbo molecular pumps, backed by a booster pump and a mechanical pump. All part numbers for the components used can be found in the Supplementary Material.

After each excitation, the chirped pulse is blocked using an SPST switch, and the FIDs collected are amplified with two low noise amplifiers (LNA) operating between 14-27 GHz and 17-27 GHz. The amplified FID is then down-converted with a second local oscillator (LO-2). The single frequency LO-2s are generated from the second channel (CH2) of the AWG, simultaneously to CH1. Each LO-2 pulse is 15 μs long, and the pulse train of LO-2s are frequency up-converted and doubled to 18-26 GHz in the same manner as the CH1 chirped pulses. Each LO-2 frequency has an offset of 400 MHz above the end or below the start of the corresponding excitation chirps. This results in a final FID frequency of 400-1200 MHz for each segment, which is then digitized on a 3.2 GS/s, PCIe high-speed digitizer card. For each segment, 10 μs of FID is collected and fast Fourier transformed. In order to frequency correct the segment to their original frequency, the up-converted LO-2 frequencies are added or subtracted from each segment, and the segments are stitched together to obtain the entire rotational spectrum from 18-26 GHz, with a resolution of $\sim$100 kHz. A more detailed discussion of the lower-cost instrument design is given in the Supplementary Material (S1-Instrument Design).

3 Results and Discussion

3.1 18-26 GHz spectrometer

In order to benchmark the execution of the new design of an 18-26 GHz spectrometer, the performance is compared to that of the first CP-FTMW instrument constructed in this frequency range originating at the University of Virginia (UVA), USA[26] through the use of hexanal. The instrument at UVA collects the entire 18-26 GHz spectrum with one chirped-pulse. Hexanal has a characteristically dense spectrum, allowing for the identification of multiple conformers, as well as isotopic species. Thus, it is a prime candidate to interrogate the performance of the spectrometer with respect to the dynamic range, frequency accuracy of the transition frequencies, and resolution.

For all of the following performance tests, the data was acquired by supersonically expanding a 0.2% hexanal in neon mixture with a backing pressure of 1 bar. One nozzle was used to obtain a total of 1.9 million acquisitions. These are the same conditions that were used in the UVA instrument, with one exception: that instrument utilized three nozzles instead of one during the course of the measurement[26]. As the signal-to-noise ratio (SNR) increases linearly with the number of nozzles, the SNR obtained from the UVA spectrometers was adjusted to take this into account for a fair comparison with the presented design.

3.1.1 Phase stability

The sensitivity that FTMW spectrometers are known for hinges around the phase stability of the instrument. This sensitivity comes from the ability to coherently average the FID signal in the time domain over many spectral acquisitions. For this, phase reproducible excitation pulses are required, and they are achieved by locking the independent components of the instrument to a low phase noise reference clock. Generally, for CP-FTMW spectrometers, a standard 10 MHz rubidium (Rb) oscillator is used[17,24,26,43,44], which cost around €3000. However, as

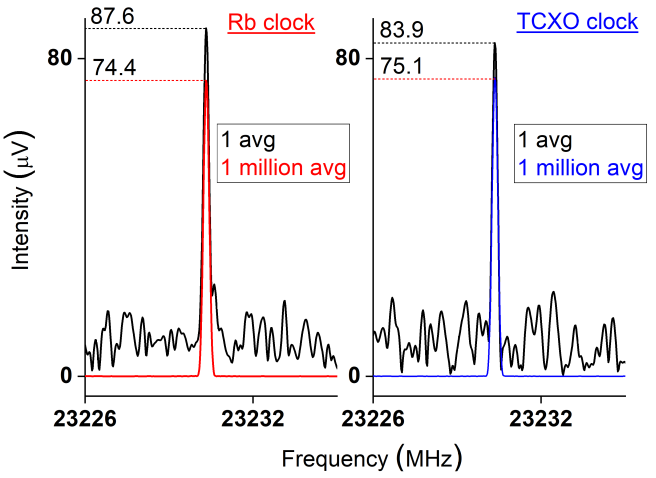

Fig. 2 A comparison between the standard rubidium clock (Rb) and the TCXO clock offered by the Valon synthesizer used as references for the 18-26 GHz instrument. Both the spectra compare the signal level for one average versus 1 million acquisition(s) for a rotational transition of conformer 1 of hexanal.

one of the aims of the design of the instrument is to reduce the cost and make the technique more attainable, alternative reference sources were considered. The Valon synthesizer, which was already integrated in the instrument's design, contains an internal temperature compensated crystal oscillator (TCXO), and thus, was a likely a candidate to replace the standard Rb clock. The phase stability of the instrument with both clocking sources was evaluated with the signal level of transitions from hexanal. Fig. 2 shows a comparison of the signal level of a transition of conformer 1 of hexanal taken with one average and 1 million averages, using a standard Rb clock or the TCXO clock offered by the Valon synthesizer as references. In both cases, the signal intensity decreases upon long averaging is approximately 10%, and this trend holds true for the rest of the spectrum. The results showcase the similar performance of both clock sources upon long averaging, and thus, the TCXO clock from the Valon synthesizer was chosen to be the reference source of the spectrometer. A more detailed discussion is given in section S2.1 of the Supplementary Material.

3.1.2 Dynamic range

As the phase stability of the instrument was demonstrated, the dynamic range was investigated in earnest. In the previous study[26], 12 conformers of hexanal were observed, and they provided an experimental relative energy ordering, with conformer 1 being the global minimum. For conformers 1-4, all ^{13}C isotopologues were assigned, with ^{18}O isotopologues being assigned for conformers 1 and 2 in natural abundance. With the segmented CP-FTMW 18-26 GHz spectrometer, all 12 conformers of hexanal were similarly identified, as shown in Fig. 3, and the same isotopologues were also observed in natural abundance.

The SNR of each conformer can be compared between spectra to benchmark the sensitivity of the spectrometer. Seifert et al.[26] obtained an effective SNR (after scaling) of ca. 1666:1 for conformers 1 and 2 and ca. 100:1 for conformers 3 and 4, while

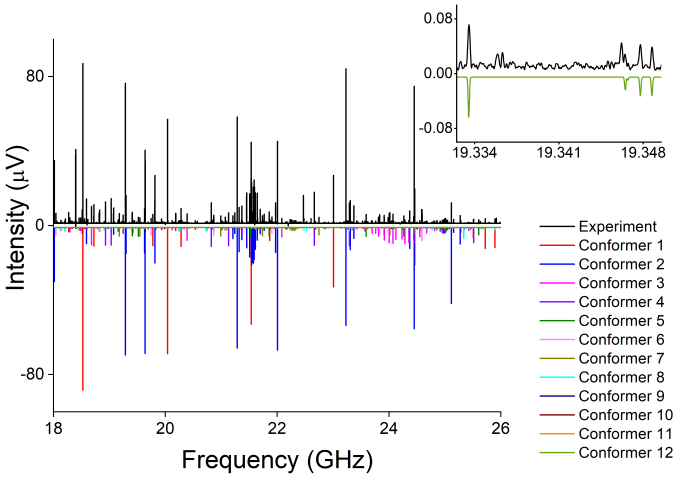

Fig. 3 The rotational spectrum of 1-hexanal measured with the segmented CP-FTMW 18-26 GHz spectrometer. The black trace shows the experimental spectrum, and the simulations of all the 12 assigned conformers based on the experimental rotational parameters are shown in color. Inset: Zoom in of the spectrum to show conformer 12, where the labelling of the x and y axes are the same as the main figure.

for the presented instrument, conformer 1 and 2 had a SNR of approximately 2330:1 and 3900:1, respectively, and conformers 3 and 4 had a SNR greater than 100:1. With these values, it can be concluded that the dynamic range of the segmented 18-26 GHz CP-FTMW spectrometer does not suffer with the implementation of this design, and the instrument can be used to measure complex systems wherein multiple conformers, isomers, and isotopologues may be present. A second example of the capabilities of this instrument can be found in section S2.2 of the Supplementary Material. The overall intensity profile obtained from the segmented 18-26 GHz CP-FTMW spectrometer, which is dependent on the temperature, carrier gas, backing pressure and valve condition, is comparable with the CP-FTMW 18-26 GHz instrument. This can be seen in Fig. S3, and it is further discussed in section S2.3 of the Supplementary Material.

3.1.3 Resolution and frequency accuracy

The resolution of the spectrometer based on the FID collection time is ∼100 kHz. After applying an apodization window, the full width at half maximum (FWHM) of line transitions is ∼240 kHz. This compares with the UVA spectrometer for the same conditions.

The frequency accuracy of the instrument has been benchmarked by comparing the center frequencies determined for all of the measured rotational transitions of conformer 1 of hexanal and its ^{18}O isotopologue obtained from the UVA 18-26 GHz CP-FTMW spectrometer[26] to those obtained from the segmented 18-26 GHz CP-FTMW spectrometer. For simplicity in the following discussion, the UVA 18-26 GHz CP-FTMW spectrometer is referred to as 'UVA', and the segmented 18-26 GHz CP-FTMW spectrometer as 'Hamburg'. The measured transitions of conformer 1 of hexanal and its ^{18}O isotopologue obtained from the UVA spectrometer were fit to an asymmetric rotational Hamiltonian to generate a set of rotational constants for each species. Along with these rotational constants, root mean square (RMS) errors, which tallies the observed minus calculated (OMC) values for the transition frequencies were obtained. From the assigned rotational transitions with the UVA spectrometer, an RMS value of ∼4 kHz and ∼7 kHz was obtained for conformer 1 of hexanal and its ^{18}O isotopologue, respectively. The fitting procedure was done for the assigned transitions from the Hamburg spectrometer, in which the rotational constants were fixed to the values that were found from the UVA spectrometer. RMS values of ∼12.7 kHz for conformer 1 and ∼17 kHz for the ^{18}O isotopologue are obtained. In this case, the individual OMC were observed to be less than 20 kHz, except for one discrepancy. The measured transitions from the Hamburg spectrometer were also fit to an asymmetric rotational Hamiltonian where the rotational constants were allowed to be fit. This resulted in RMS values of ∼6 kHz for conformer 1 of hexanal and ∼9 kHz for its ^{18}O isotopologue. Here, the difference between the measured and calculated frequency values is below 10 kHz, for both species. A summary of the fits is given in Table S1 and their corresponding transitions are given in Tables S6-S7 of the Supplementary Material. The deviation in the A, B, and C rotational constants from the Hamburg spectrometer compared to those from the UVA spectrometer is less than 0.001%

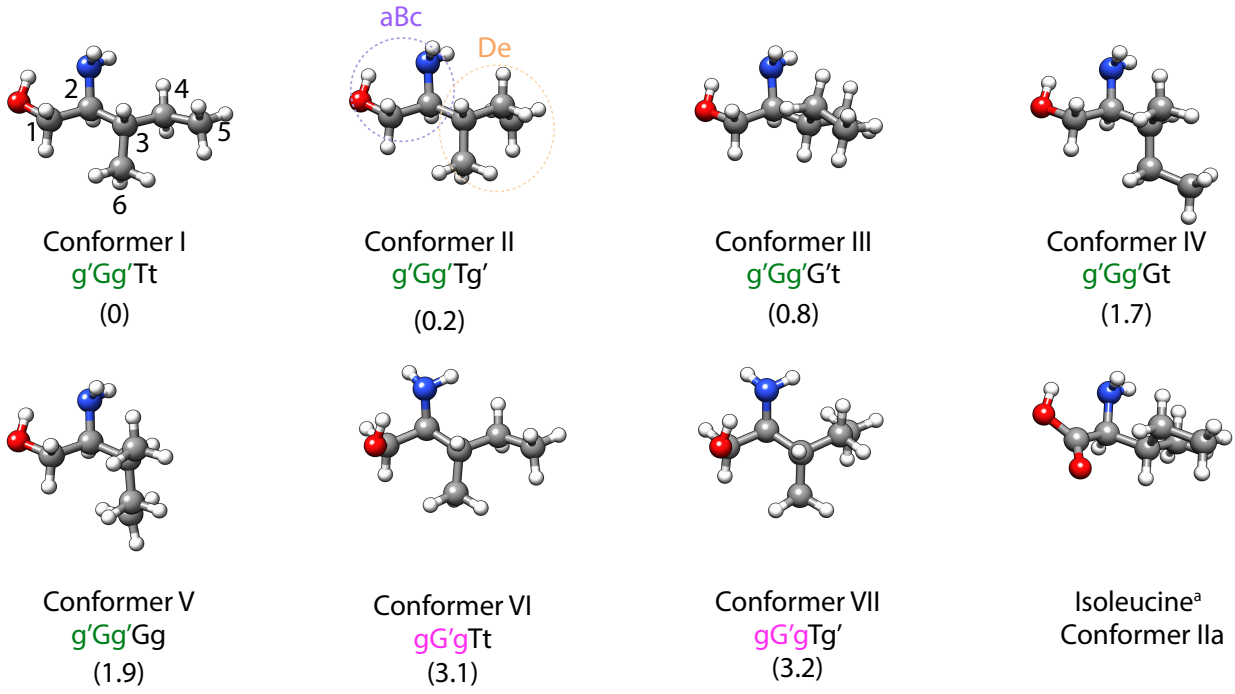

Fig. 4 The seven lowest energy conformers of L-isoleucinol calculated at the B3LYP/aug-cc-pVTZ level of theory. The values in parentheses are zero point corrected relative energies with respect to the lowest energy structure, Conformer I (g'Gg'Tt), in kJ mol^{-1}. Conformer I shows the labelling for carbon atom numbers, and the colored circles on Conformer II show the division of dihedral angles into the amino alcohol group 'aBc' and the side chain 'De' (see text). [a] Figure of isoleucine (Conformer IIa$_1$) adapted from Lesarri et al.[45] is shown for comparison.

in both cases. The RMS values of the Hamburg spectrometer closely matches to the UVA spectrometer. This, along with the example presented in the Supplementary Material section S2.4 for carbonyl sulfide, shows that the frequency accuracy is comparable to the broadband design. A complete discussion on the cost and performance of the instrument is given in sections S3 of the Supplementary Material.

3.2 Theoretical predictions and conformational search of isoleucinol

The conformational search with Spartan and the re-optimization of the structures with the B3LYP-D3(BJ)/def2-TZVP and B3LYP/aug-cc-pVTZ levels of theories resulted in seven conformers of L-isoleucinol that were within 6 kJ mol^{-1} of the lowest energy conformer, as shown in Fig. 4. The energy cut-off at 6 kJ mol^{-1} was chosen based on the observation of a previously studied flexible molecule citronellal, which was investigated under similar experimental conditions[46]. The next higher energy structure of isoleucinol at the B3LYP-D3(BJ)/def2-TZVP is at 6.8 kJ mol^{-1} from the global minimum and will be addressed later in the paper. The large conformational flexibility of isoleucinol arises from the different possible orientations of the five aliphatic dihedral angles, namely lonepair(lp)-N-C2-C1, N-C2-C1-O, C2-C1-O-H, C1-C2-C3-C4, and C2-C3-C4-C5. The atom numbering can be found in Fig. 4. The structures are named based on the dihedral angles and can be grouped in two parts, as shown in Fig. 4: 'aBc' for the three dihedral angles of the amino alcohol group and 'De' for the two dihedral angles of the *sec*-butyl side chain (R = -CH(CH$_3$)CH$_2$CH$_3$). The amino alcohol group is comprised of NH$_2$-CH$_2$-CH$_2$-OH, and it is similar to the side chain of an already-studied amino alcohol, alaninol[21], in which R = CH$_3$. The dihedral angles 'aBc' are a = lp-N-C2-C1, B = N-C2-C1-O, and c = C2-C1-O-H, and they can take three possible conformations – around 180° (trans, or T/t), 60° (gauche, or G/g) or -60° (gauche, or G'/g'). The side chain 'De' is further defined by the three possible conformations of the *sec*-butyl dihedrals, where D = C1-C2-C3-C4 and e = C2-C3-C4-C5. As each of the five dihedral angles can have three possible orientations, a total of 3^5(=243) different structures for isoleucinol could be possible.

In all seven structures, the amino alcohol dihedral 'aBc' moiety takes on one of the two orientations observed in alaninol[21]. For Conformers I-V, the 'aBc' arrangement corresponds to the one found in Conformer I of alaninol (g'Gg'), and for Conformers VI and VII, it corresponds to that of alaninol Conformer II (gG'g). For each amino alcohol backbone the two dihedrals 'D' and 'e' can take on nine possible conformations: Tt, Tg, Tg', Gt, Gg, Gg', G't, G'g, and G'g'. Among these, the conformational possibilities Tg, Gg', G'g and G'g' were predicted to be higher than the conformational possibilities Tt, Tg', Gt, Gg and G't, as they would have steric hindrance between the C5 carbon and the C2/NH$_2$ groups of the amino alcohol backbone. The five lowest energy possibilities of the 'De' configuration for the g'Gg amino alcohol backbone are shown in Fig. 4. For conformers with an amino alcohol back-

Table 1 A comparison of the experimental and theoretical rotational constants (A, B, C), quartic centrifugal distortion constants (D_J, D_{JK}, D_K, δ_J, δ_K), and nitrogen nuclear quadrupole coupling constants (χ_{aa}, χ_{bb} - χ_{cc}) for the seven conformers of isoleucinol at the B3LYP/aug-cc-pVTZ level of theory.

	Conformer I G'Gg'Tt		Conformer II G'Gg'Tg'		Conformer III G'Gg'G't		Conformer IV G'Gg'Gt	
	Experiment	B3LYP	Experiment	B3LYP	Experiment	B3LYP	Experiment	B3LYP
A (MHz)	3759.34376(39)	3749.7	3067.56626(32)	3075.1	3170.22321(33)	3154.6	3234.58882(34)	3219.6
B (MHz)	1062.44909(12)	1056.9	1213.42566(16)	1196.8	1103.61682(17)	1094.1	1083.52381(21)	1076.7
C (MHz)	880.24579(13)	875.2	1010.54858(14)	999.0	971.59291(15)	965.6	972.62991(22)	964.3
D_J (kHz)	0.02663(55)		0.11429(88)		0.08475(84)		0.0881(11)	
D_{JK} (kHz)	0.3348(82)		−0.2067(55)		0.3651(58)		−0.2216(76)	
D_K (kHz)	–		–		–		2.158(17)	
δ_J (kHz)	–		0.02256(63)		0.01271(62)		0.02247(55)	
δ_K (kHz)	–		–		–		1.036(71)	
χ_{aa} *1.5 (MHz)	−6.3228(46)	−7.02	−5.2345(49)	−5.89	−6.3234(50)	−7.01	−5.5288(45)	−6.10
(χ_{bb} - χ_{cc})*0.25 (MHz)	0.1242(15)	0.11	0.1195(15)	0.13	−0.1286(15)	−0.11	0.0405(15)	−0.02
μ_a /D		3.2		3.0		2.9		2.4
μ_b /D		1.0		0.6		1.0		2.0
μ_c /D		0.5		1.3		0.8		0.4
Number of lines (*a*/*b*/*c*)	357 (y/y/y)		269 (y/y/y)		323 (y/y/y)		278 (y/y/y)	
σ (kHz)	12.5		11.2		11.4		11.0	

	Conformer V G'Gg'Gg		Conformer VI gG'gTt		Conformer VII gG'gTg'	
	Experiment	B3LYP	Experiment	B3LYP	Experiment	B3LYP
A (MHz)	2357.79993(38)	2377.5	3124.11041(36)	3132.4	3000.70059(60)	3022.3
B (MHz)	1370.35475(21)	1326.6	1218.15680(11)	1202.7	1332.57586(26)	1307.3
C (MHz)	1107.69103(20)	1095.3	1019.16409(12)	1007.9	1089.86075(21)	1072.8
D_J (kHz)	0.4981(18)		0.10863(65)		0.1316(12)	
D_{JK} (kHz)	−1.377(10)		–		–	
D_K (kHz)	1.797(20)		0.495(38)		–	
δ_J (kHz)	0.20951(91)		0.00966(26)		0.03128(91)	
δ_K (kHz)	0.970(24)		–		–	
χ_{aa} *1.5 (MHz)	−4.5597(49)	−5.13	0.8771(38)	1.07	−0.6530(60)	−0.73
(χ_{bb} - χ_{cc})*0.25 (MHz)	−0.2174(18)	−0.29	1.2566(11)	1.39	1.1084(17)	1.18
μ_a /D		2.3		1.5		2.1
μ_b /D		2.0		1.7		1.4
μ_c /D		1.0		1.6		1.1
Number of lines (*a*/*b*/*c*)	272 (y/y/y)		323 (y/y/y)		154 (y/y/y)	
σ (kHz)	11.2		10.3		10.5	

bone arrangement of gG'g, 'De' configurations other than Tt and Tg' are higher than 6 kJ mol^{-1} relative to Conformer I and are not discussed further. It is interesting to note the similarity in conformers I and VI, where the dihedral 'De' is Tt. The side chain R is planar and minimizes steric hindrance. The next pair of conformers, II and VII, are also similar in this way.

As isoleucinol is a potential precursor to isoleucine, it is interesting to compare the structural relation between these two molecules. A previous study on isoleucine[45] predicts 10 different structures at MP2/6-311g++(d,p) within 6 kJ mol^{-1}. From these, two structures differing by 1.7 kJ mol^{-1} were observed experimentally using FTMW spectroscopy[45]. In these two structures of isoleucine, the configuration of the amino acid is dominated by the intramolecular hydrogen bond N-H$\cdots$O=C for Conformer Ia_1 and by an N$\cdots$H-O interaction for Conformer IIa_1. Because of the absence of the carbonyl group in isoleucinol, only an analog of the second observed conformer of isoleucine should be observed, as shown in Fig. 4. In both conformers of isoleucine, the dihedral angles 'De' are in the G't configuration. The Tt or Tg' configurations, which are present in the lowest energy forms of isoleucinol, are not expressed in any of the predicted 10 conformations of isoleucine. This could be explained based on the carboxylation of the C1 carbon atom of isoleucinol. The carboxyl group and the C4/C6 atoms in isoleucine will have steric hindrance, which prefers the dihedral 'D' to be in the G' configuration.

3.3 Experimental analysis of isoleucinol

In our data, we were able to assign all seven conformers of L-isoleucinol predicted to be within 6 kJ mol^{-1} of the global minimum. The next higher energy structure, which has a μ_a dipole moment component of 3.3 D, was searched for in the spectra; however, it remains untraceable, agreeing well with the 6 kJ mol^{-1} energy cut-off. Fig. 5 shows the spectrum recorded with the segmented 18-26 GHz CP-FTMW spectrometer (top trace in black) compared with the simulated spectra of the fitted rotational constants (bottom traces in color). In the frequency range from 2-26 GHz, hyperfine splitting was observed, as shown in the inset of Fig. 5. This splitting structure is a result of the coupling of the ^{14}N nuclear spin I=1 with the molecular rotational angular momentum J and gives rise to a total angular momentum of the molecule F, where $F = J+I, J+I-1, J+I-2, \ldots, |J-I|$. Analysis of this hyperfine structure provides nuclear quadrupole coupling constants. The fits for the seven conformers are given in Table 1, including the nitrogen quadrupole coupling parameters (χ_{aa}, χ_{bb} - χ_{cc}). A comparison to the predicted values at the B3LYP/aug-cc-

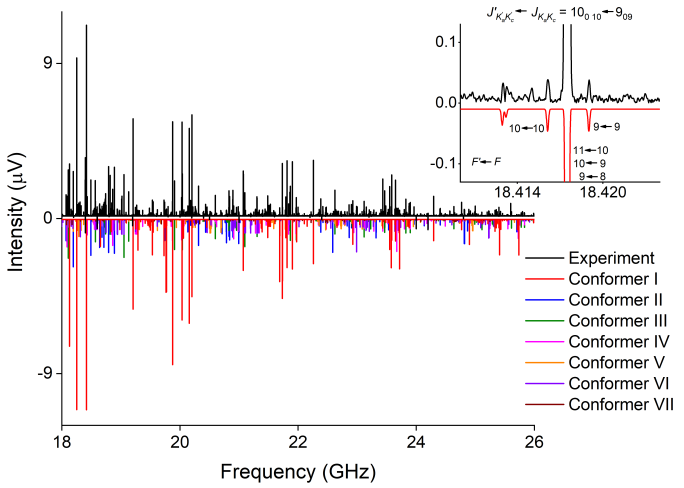

Fig. 5 The spectrum of isoleucinol recorded with the 18-26 GHz segmented CP-FTMW spectrometer. The top, black trace shows the experimental spectrum, and the simulations of the seven assigned conformers based on the fitted rotational parameters are given on the bottom at 1.5 K (multicolored). Inset: Nuclear quadrupole coupling hyperfine structure for the $10_{010} \leftarrow 9_{09}$ rotational transition due to the ^{14}N nucleus, with F quantum numbers.

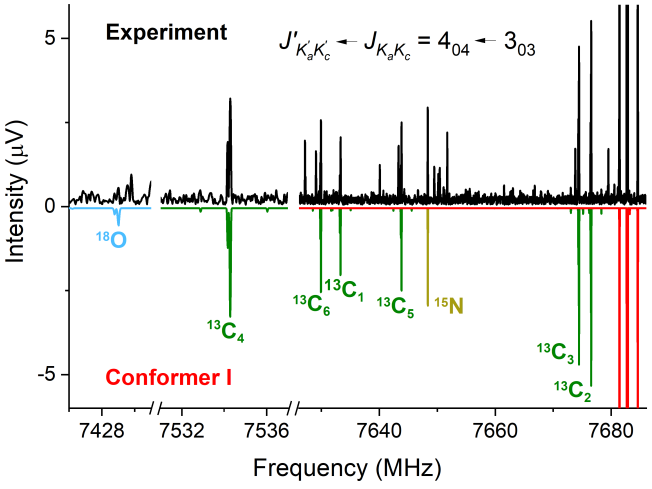

Fig. 6 Parts of the spectrum of isoleucinol, highlighting the measured isotopologues in natural abundance with the Hamburg COMPACT spectrometer. The top, black trace shows the experimental spectrum, with the simulations of the assigned ^{13}C (green), ^{15}N (yellow) and ^{18}O (cyan) isotopologues for the $J'_{K_a'K_c'} \leftarrow J_{K_aK_c} = 4_{04} \leftarrow 3_{03}$ transition of Conformer I (red) on the bottom.

pVTZ level of theory is also presented. A linelist for all the seven conformers from 2-26 GHz are given in Tables S8-S14.

The most intense lines in the 2-26 GHz spectra belong to the global minimum, Conformer I, followed by Conformer II-VII, respectively, agreeing well with the zero point corrected energy ordering obtained at the B3LYP/aug-cc-pVTZ level of theory (Fig. 4). For all of the observed conformers, the quantum chemical calculation values lie within 3% of the experimental rotational constants (Table 1). The magnitude of the calculated dipole moments are in agreement with the type of observed transitions (*a*-, *b*-, or *c*- type) for each conformer.

3.4 Experimental structure of Conformers I and II of isoleucinol

In the experimental spectrum, the SNR was sufficient to observe single ^{13}C isotopic substitutions in natural abundance (1.1%) for Conformers I and II. For the global minimum Conformer I, ^{18}O and ^{15}N isotopologues were also assigned, which have a natural abundance of 0.2% and 0.4%, respectively. Note that hyperfine splitting is absent in ^{15}N isotopologues as the spin of the ^{15}N nucleus is I=1/2. The analysis of the isotopologues provides us with accurate structural information, further confirming our conformer assignment. Fig. 6 shows the assignment of the isotopologues' transitions in the 2-8 GHz spectrum for the $J'_{K_a'K_c'} \leftarrow J_{K_aK_c} = 4_{04} \leftarrow 3_{03}$ transition of Conformer I. To obtain the experimental fit for the rare isotopologues, the centrifugal distortion constants and quadrupole coupling constants were fixed to the parent species values. A summary of the fitted rotational constants and observed frequencies of the ^{13}C, ^{18}O and ^{15}N isotopologues are given in Tables S4, S5, and S15-S28. From this data, the Kraitchman equations[27] were used to determine a heavy atom substitution (r_s) structure for Conformer I and the carbon backbone for Conformer II. This method determines the magnitudes of the coordinates for each substituted atom from the rotational constants of the isotopologues without information from quantum-chemical calculations, and it does not consider any structural changes due to isotopic substitution. The theoretical results are only used to guide the sign of each coordinate. Fig. 7 shows a comparison between the r_s structures and the B3LYP/aug-cc-pVTZ results for

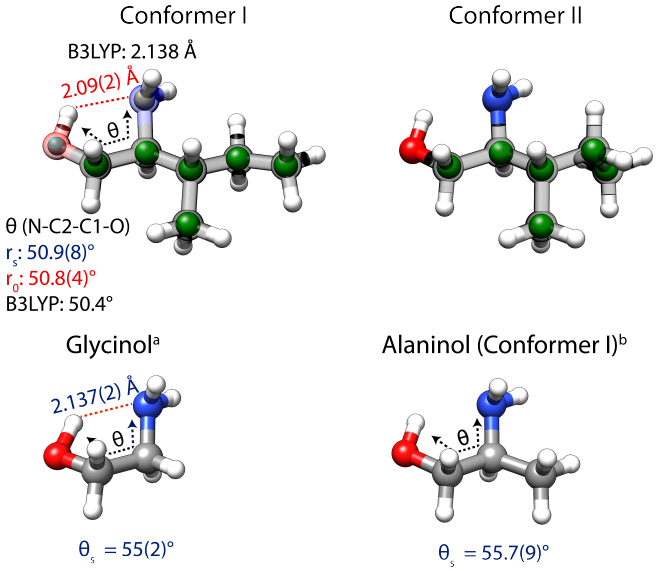

Fig. 7 The r_s (blue) and r_0 (red) experimental structures of Conformer I (g'Gg'Tt) and Conformer II (g'Gg'Tg') of isoleucinol. The relevant experimental structural parameters, hydrogen bond distance N···H and dihedral angle N-C2-C1-O, obtained from the r_0 fit for Conformer I are compared with the results of quantum chemical calculations (B3LYP/aug-cc-pVTZ level), the experimental r_s structure of glycinol and alaninol (Conformer I). [a] adapted from Penn et al.[20] [b] adapted from Arenas et al.[23]

Conformers I and II. The r_s structure for Conformer I allowed for the determination of the experimental amino alcohol dihedral angle (θ) N-C2-C1-O = 50.9(8)°, which is compared with the quantum chemical calculation, as shown in Fig. 7. As there is no isotopologue information for the hydroxyl hydrogen, the r_s structure could not be used to evaluate the N···H bond distance. Further, this method has limited reliability in the case of determining H atom positions due to the large mass difference between H to D. To determine the experimental N···H = 2.09(2) Å bond distance, a least squares fit was instead performed. This method involves fitting the effective ground state structure, r_0, with the 27 rotational constants [three times one (parent), three times six (^{13}C atoms), three times one (^{18}O atom), and three times one (^{15}N atom)] obtained from the isotopologues of Conformer I. The primary parameters of the fit were O-H and C-C bond distances, angles, and dihedral angles. The resulting coordinates from this were then fed into the EVAL program, which calculates bond distances, angles, and dihedral angles from the input coordinates.

No experimental structural information is available for the second conformer of isoleucine, Conformer IIa$_1$ [45], which is comparable with the structures of isoleucinol. There is, however, an experimental N···H-O hydrogen bond distance reported for the smaller amino acid alanine. Similar to isoleucine, two structures of alanine have been observed with rotational spectroscopy [47], having the intramolecular hydrogen bond N-H···O=C for Conformer I and an N···H-O interaction for Conformer IIa. Because of the absence of the carbonyl group, isoleucinol can only be compared with Conformer IIa of alanine. For alanine, the N···H hydrogen bond distance determined with the least squares fit (r_0) method is reported to be 1.96(1) Å. This is slightly less than for isoleucinol (2.09(2) Å). A plausible reason for this hydrogen bond elongation is the difference in the θ NCCO, which is -11.5(8)° for alanine and 50.8(4)° for isoleucinol. The difference is due to the C1 carbon being sp^2 hybridized in alanine and sp^3 in isoleucinol.

The experimental parameters of Conformer I of isoleucinol can be compared with its analogous amino alcohols, like glycinol [20] and alaninol [21,23]. The experimental structures of these molecules have been determined using rotational spectroscopy. The available structural parameters for glycinol allow for a comparison of the amino alcohol backbone structure, using the N···H-O hydrogen bond distance and the dihedral angle N-C2-C1-O (Fig. 7). In glycinol, the N···H hydrogen bond distance and dihedral angle within the r_s structure are reported to be 2.137(2) Å and 55(2)°, respectively, and they are similar to isoleucinol's hydrogen bond distance of 2.09(2) Å and dihedral angle of 50.8(4)°. With Conformer I of alaninol, the experimental structure only allowed for a comparison of the dihedral angle, which in the recent study by Arenas et al. [23] is 55.7(9)° and closely matches the dihedral angle of Conformer I of isoleucinol. This similarity shows that the amino alcohol backbone remains the same when increasing the size of the amino alcohol. The only structural change is due to the orientation of the *sec*-butyl side group R.

The agreement between theory and experiment is evident from the comparison of the two structures for Conformers I and II (Fig. 7). A comparison with alanine, isoleucine, glycinol, and alaninol further confirms that there is little-to-no interaction between the amino alcohol group and the side chain R.

4 Conclusion and Outlook

High-resolution broadband rotational spectroscopy between 2-26 GHz was used to successfully observe seven conformers of isoleucinol, a potential precursor to an essential amino acid of astrochemical relevance. In the observed conformers, the amino alcohol backbone collapsed to the two structures observed for alaninol [21], g'Gg' (Conformer I) and gG'g (Conformer II), and the structural flexibility lies in the *sec*-butyl side chain. It was seen that in these conformers of isoleucinol there is little-to-no interaction between the amino alcohol group and the side chain. In the two lowest energy conformers of isoleucinol, the presence of the isotopologues in natural abundance allowed the determination of the experimental structures. For Conformer I, the experimental intramolecular N···H-O hydrogen bond was determined to be 2.09(2) Å, and amino alcohol dihedral angle to be 50.8(4)° from the r_0 least square fit. These values are comparable to the values found in the previously studied amino alcohols glycinol and alaninol. The analysis of these seven ground-state conformers will help astronomers to search for this molecule in the ISM. If Conformer I of isoleucinol is detected in the ISM, it could indicate that isoleucine is also present in that region of the ISM, as carboxylation of isoleucinol could result in either of the two stable forms of isoleucine.

This work also establishes the development and performance of a lower-cost newly-designed segmented 18-26 GHz chirped-pulse spectrometer in Hamburg. The performance of the instrument with respect to phase stability, sensitivity, dynamic range as well as frequency accuracy and resolution was found to be comparable to the existing chirped-pulse 18-26 GHz microwave spectrometer design. The implementation of this design has reduced the cost of the instrument by half, opening its applications up to research groups or in teaching laboratories while relieving them of the burden of investing in expensive components.

Conflicts of interest

There are no conflicts to declare.

Acknowledgements

This work has been supported by the ERC Starting Grant ASTROROT (Grant Agreement Number 638027). M.F. and B.E.A acknowledge the support from the International Max Planck Research School for Ultrafast Imaging and Structural Dynamics, IMPRS-UFAST. A.L.S. acknowledges the support of the Louise Johnson Fellowship from CUI. M. F. acknowledges Sébastien Gruet for his help and insightful discussion while building the 18-26 GHz instrument.

References

1 B. A. McGuire, *The Astrophysical Journal Supplement Series*, 2018, **239**, 17.

2 I. W. Smith, *Annual Review of Astronomy and Astrophysics*, 2011, **49**, 29–66.

3 E. Herbst and J. T. Yates, *Chemical Reviews*, 2013, **113**, 8707–8709.

4 B. A. McGuire, P. B. Carroll and R. T. Garrod, *Astronomical Society of the Pacific, Conference Series*, 2018, **Monograph 7**, 245–248.

5 E. F. v. Dishoeck, *Proceedings of the International Astronomical Union*, 2017, **13**, 3–22.

6 L. M. Barge, *Nature Communications*, 2018, **9**, 1–3.

7 L. M. Ziurys, G. R. Adande, J. L. Edwards, D. R. Schmidt, D. T. Halfen and N. J. Woolf, *Origins of Life and Evolution of Biospheres*, 2015, **45**, 275–288.

8 J. M. Hollis, F. J. Lovas and P. R. Jewell, *The Astrophysical Journal*, 2000, **540**, L107–L110.

9 K. Altwegg, H. Balsiger, A. Bar-Nun, J.-J. Berthelier, A. Bieler, P. Bochsler, C. Briois, U. Calmonte, M. R. Combi, H. Cottin, J. De Keyser, F. Dhooghe, B. Fiethe, S. A. Fuselier, S. Gasc, T. I. Gombosi, K. C. Hansen, M. Haessig, A. Jäckel, E. Kopp, A. Korth, L. Le Roy, U. Mall, B. Marty, O. Mousis, T. Owen, H. Rème, M. Rubin, T. Sémon, C.-Y. Tzou, J. Hunter Waite and P. Wurz, *Science Advances*, 2016, **2**, e1600285.

10 L. E. Snyder, F. J. Lovas, J. M. Hollis, D. N. Friedel, P. R. Jewell, A. Remijan, V. V. Ilyushin, E. A. Alekseev and S. F. Dyubko, *The Astrophysical Journal*, 2005, **619**, 914.

11 P. A. Jones, M. R. Cunningham, P. D. Godfrey and D. M. Cragg, *Monthly Notices of the Royal Astronomical Society*, 2007, **374**, 579–589.

12 M. R. Cunningham, P. A. Jones, P. D. Godfrey, D. M. Cragg, I. Bains, M. G. Burton, P. Calisse, N. H. M. Crighton, S. J. Curran, T. M. Davis, J. T. Dempsey, B. Fulton, M. G. Hidas, T. Hill, L. Kedziora-Chudczer, V. Minier, M. B. Pracy, C. Purcell, J. Shobbrook and T. Travouillon, *Monthly Notices of the Royal Astronomical Society*, 2007, **376**, 1201–1210.

13 Y.-J. Kuan, S. B. Charnley, H.-C. Huang, W.-L. Tseng and Z. Kisiel, *The Astrophysical Journal*, 2003, **593**, 848.

14 H. Møllendal, L. Margulès, A. Belloche, R. A. Motiyenko, A. Konovalov, K. M. Menten and J. C. Guillemin, *Astronomy & Astrophysics*, 2012, **538**, A51.

15 S. L. Miller, *Journal of the American Chemical Society*, 1955, **77**, 2351–2361.

16 S. Maeda and K. Ohno, *The Astrophysical Journal*, 2006, **640**, 823.

17 G. G. Brown, B. C. Dian, K. O. Douglass, S. M. Geyer, S. T. Shipman and B. H. Pate, *Review of Scientific Instruments*, 2008, **79**, 053103.

18 J. L. Neill, B. J. Harris, A. L. Steber, K. O. Douglass, D. F. Plusquellic and B. H. Pate, *Optics Express*, 2013, **21**, 19743–19749.

19 B. E. Arenas, S. Gruet, A. L. Steber, B. M. Giuliano and M. Schnell, *Physical Chemistry Chemical Physics*, 2017, **19**, 1751–1756.

20 R. E. Penn and R. F. Curl, *The Journal of Chemical Physics*, 1971, **55**, 651–658.

21 B. H. Ellingsen, K. M. Marstokk and H. Møllendal, *Journal of Molecular Structure*, 1978, **48**, 9–23.

22 D. Loru, I. Peña, J. L. Alonso and M. E. Sanz, *Chemical Communications*, 2016, **52**, 3615–3618.

23 C. P. S. F. A. L. S. Benjamin E. Arenas, Mariyam Fatima and M. Schnell, *Astronomy and Astrophysics*, 2020, Submitted.

24 D. Schmitz, V. Alvin Shubert, T. Betz and M. Schnell, *Journal of Molecular Spectroscopy*, 2012, **280**, 77–84.

25 C. Pérez, A. Krin, A. L. Steber, J. C. López, Z. Kisiel and M. Schnell, *The Journal of Physical Chemistry Letters*, 2016, **7**, 154–160.

26 N. A. Seifert, I. A. Finneran, C. Perez, D. P. Zaleski, J. L. Neill, A. L. Steber, R. D. Suenram, A. Lesarri, S. T. Shipman and B. H. Pate, *Journal of Molecular Spectroscopy*, 2015, **312**, 13–21.

27 D. F. Plusquellic, R. D. Suenram, B. Maté, J. O. Jensen and A. C. Samuels, *JChPh*, 2001, **115**, 3057–3067.

28 C. M. Western, *Journal of Quantitative Spectroscopy and Radiative Transfer*, 2017, **186**, 221–242.

29 Z. Kisiel, L. Pszczółkowski, I. R. Medvedev, M. Winnewisser, F. C. De Lucia and E. Herbst, *Journal of Molecular Spectroscopy*, 2005, **233**, 231–243.

30 Z. Kisiel, L. Pszczółkowski, B. J. Drouin, C. S. Brauer, S. Yu, J. C. Pearson, I. R. Medvedev, S. Fortman and C. Neese, *Journal of Molecular Spectroscopy*, 2012, **280**, 134–144.

31 J. Kraitchman, *American Journal of Physics*, 1953, **21**, 17–24.

32 Z. Kisiel, *Journal of Molecular Spectroscopy*, 2003, **218**, 58–67.

33 `http://www.ifpan.edu.pl/~kisiel/prospe.htm`.

34 `https://www.wavefun.com/research`.

35 A. D. Becke, *The Journal of Chemical Physics*, 1993, **98**, 5648–5652.

36 S. Grimme, J. Antony, S. Ehrlich and H. Krieg, *The Journal of Chemical Physics*, 2010, **132**, 154104.

37 S. Grimme, S. Ehrlich and L. Goerigk, *Journal of Computational Chemistry*, 2011, **32**, 1456–1465.

38 F. Weigend and R. Ahlrichs, *Physical Chemistry Chemical Physics*, 2005, **7**, 3297–3305.

39 M. J. Frisch, G. W. Trucks, H. B. Schlegel, G. E. Scuseria, M. A. Robb, J. R. Cheeseman, G. Scalmani, V. Barone, B. Mennucci, G. A. Petersson, H. Nakatsuji, M. Caricato, X. Li, H. P. Hratchian, A. F. Izmaylov, J. Bloino, G. Zheng, J. L. Sonnenberg, M. Hada, M. Ehara, K. Toyota, R. Fukuda, J. Hasegawa, M. Ishida, T. Nakajima, Y. Honda, O. Kitao, H. Nakai, T. Vreven, J. A. Montgomery, Jr., J. E. Peralta, F. Ogliaro, M. Bearpark, J. J. Heyd, E. Brothers, K. N. Kudin, V. N. Staroverov, R. Kobayashi, J. Normand, K. Raghavachari, A. Rendell, J. C. Burant, S. S. Iyengar, J. Tomasi, M. Cossi, N. Rega, J. M. Millam, M. Klene, J. E. Knox, J. B. Cross, V. Bakken, C. Adamo, J. Jaramillo, R. Gomperts, R. E. Stratmann, O. Yazyev, A. J. Austin, R. Cammi, C. Pomelli, J. W. Ochterski, R. L. Martin, K. Morokuma, V. G. Zakrzewski, G. A. Voth, P. Salvador, J. J. Dannenberg, S. Dapprich, A. D. Daniels, Ö. Farkas, J. B. Foresman, J. V. Ortiz, J. Cioslowski and D. J. Fox, *Gaussian 09 Revision E.01*, Gaussian Inc. Wallingford CT 2009.

40 T. H. Dunning, *The Journal of Chemical Physics*, 1989, **90**, 1007–1023.

41 D. E. Woon and T. H. Dunning, *The Journal of Chemical*

Physics, 1993, **98**, 1358–1371.

42 R. A. Kendall, T. H. Dunning and R. J. Harrison, *The Journal of Chemical Physics*, 1992, **96**, 6796–6806.

43 D. P. Zaleski, S. L. Stephens and N. R. Walker, *Physical Chemistry Chemical Physics*, 2014, **16**, 25221–25228.

44 D. P. Zaleski, J. L. Neill, M. T. Muckle, N. A. Seifert, P. Brandon Carroll, S. L. Widicus Weaver and B. H. Pate, *Journal of Molecular Spectroscopy*, 2012, **280**, 68–76.

45 A. Lesarri, R. Sánchez, E. J. Cocinero, J. C. López and J. L. Alonso, *Journal of the American Chemical Society*, 2005, **127**, 12952–12956.

46 S. R. Domingos, C. Pérez, C. Medcraft, P. Pinacho and M. Schnell, *Physical Chemistry Chemical Physics*, 2016, **18**, 16682–16689.

47 S. Blanco, A. Lesarri, J. C. López and J. L. Alonso, *Journal of the American Chemical Society*, 2004, **126**, 11675–11683.